Tunable one-dimensional photonic crystal slabs based on preferential etching of silicon-on-insulator

D. C. Zografopoulos and E. E. Kriezis

Department of Electrical and Computer Engineering, Aristotle University of Thessaloniki, Thessaloniki GR-54124, Greece.

dzogra@auth.gr, mkriezis@auth.gr

B. Bellini and R. Beccherelli

Consiglio Nazionale delle Ricerche - Istituto per la Microelettronica e Microsistemi (CNR-IMM), 00133 Rome, Italy

robert.bellini@imm.cnr.it, romeo.beccherelli@imm.cnr.it

Abstract: We design and assess a one-dimensional photonic crystal slab fabricated by preferential etching of a silicon-on-insulator substrate. The etched grooves are considered to be infiltrated by a highly-birefringent nematic liquid crystalline material. A detailed analysis of the nematic director response within the grooves is presented. We investigate different configurations and demonstrate large band gap shifting when switching the liquid crystal with an applied voltage. Furthermore, we assess this type of device as an efficient alternative for compact refractometric optical sensing applications.

OCIS codes: (250.0250) Optoelectronics; (230.3990) Microstructure devices; (230.3720) Liquid crystal devices; (050.2770) Gratings.

References and links

1. C. Weisbuch, E. Schwoob, S. Olivier, H. Benisty, A. Talneau, G.-H. Duan, T. F. Krauss, C. J. M. Smith, R. Houdré, R. Ferrini, and M. Agio, "Towards real-world devices in InP-based PCs," Proc. SPIE **5360**, 77–90 (2004).
2. "Photonic crystals and related photonic nanostructures," Jap. J. Appl. Phys. **45**, Part 1 (8A) (2006).
3. M. Bertolotti, "Wave interactions in photonic band structures: an overview," J. Opt. A: Pure Appl. Opt. **8**, S9–S32 (2006).
4. A.M. Merzlikin and A.P. Vinogradov, "Superprism effect in 1D photonic crystal," Opt. Commun. **259**, 700–703 (2006).
5. D. Yudistira, H.J.W.M. Hoekstra, M. Hammer, and D.A.I. Marpaung, "Slow light excitation in tapered 1D photonic crystals: theory," Opt. Quantum Electron. **38**, 161–176 (2006).
6. G.P. Wang, Y. Yi, and W. Lin, "Tunable and omnidirectional photonic bandgap properties of one-dimensional photonic crystals fabricated by holography," J. Opt. Soc. Am. B **21**, 554–561 (2004).
7. R. Ozaki, M. Ozaki, and K. Yoshino, "Defect mode in one-dimensional photonic crystal with in-plane switchable nematic liquid crystal defect layer," Jap. J. Appl. Phys., **43**, L1477–L1479 (2004).
8. V.A. Tolmachev, E.V. Astrova, J.A. Pilyugina, T.S. Perova, R.A. Moore, and J.K. Vij, "1D photonic crystal fabricated by wet etching of silicon," Opt. Mater. **27**, 831–835 (2005).
9. J. Čtyroký, S. Helfert, R. Pregla, P. Bienstman, R. Baets, R. De Ridder, R. Stoffer, G. Klaasse, J. Petráček, P. Lalanne, J.-P. Hugonin, and R.M. De La Rue, "Bragg waveguide grating as a 1D photonic band gap structure: COST 268 modelling task," Opt. Quantum Electron. **34**, 455–470 (2002).
10. D. Gerace and L.C. Andreani, "Gap maps and intrinsic diffraction losses in one-dimensional photonic crystal slabs," Phys. Rev. E **69**, 056603 (2004).

#77781 - $15.00 USD Received 4 December 2006; revised 17 January 2007; accepted 18 January 2007

11. W. Bogaerts, R. Baets, P. Dumon, V. Wiaux, S. Beckx, D. Taillaert, B. Luyssert, J. Van Campenhout, P. Bienstman, and D. Van Thourhout, "Nanophotonic waveguides in silicon-on-insulator fabricated with CMOS technology," J. Lightwave Technol. **23**, 401–412 (2005).
12. R. Ferrini, R. Houdré, H. Benisty, M. Qiu, and J. Moosburger, "Radiation losses in planar photonic crystals: two-dimensional representation of hole depth and shape by an imaginary dielectric constant," J. Opt. Soc. Am. B **20**, 469–478 (2003).
13. Y. Tanaka, T. Asano, Y. Akahane, B.-S. Song, and S. Noda, "Theoretical investigation of a two-dimensional photonic crystal slab with truncated cone air holes," Appl. Phys. Lett. **82**, 1661–1663 (2003).
14. J. Haneveld, H. Jansen, E. Berenschot, N. Tas, and M. Elwenspoek, "Wet anisotropic etching for fluidic 1D nanochannels," J. Micromech. Microeng. **13**, S62–S66 (2003).
15. A.S. Holmes, "Microengineering: the next revolution?," available on: http://www3.imperial.ac.uk/portal/pls/portallive/docs/1/185938.PDF
16. L. De Stefano, K. Malecki, M. Rossi, L. Rotiroti, F.G. Della Corte, L. Moretti, and I. Rendina, "Integrated silicon-glass opto-chemical sensors for lab-on-chip applications," Sens. Actuators B **114**, 625–630 (2006).
17. B. Bellini, J.-F. Larchanché, J.-P. Vilcot, D. Decoster, R. Beccherelli, and A. d'Alessandro, "Photonic devices based on preferential etching," Appl. Opt. **44**, 7181–7186 (2005).
18. B. Wild, R. Ferrini, R. Houdré, M. Mulot, S. Anand, and C. J. M. Smith, "Temperature tuning of the optical properties of planar photonic crystal microcavities," Appl. Phys. Lett. **84**, 846–848 (2004).
19. R. Ferrini, J. Martz, L. Zuppiroli, B. Wild, V. Zabelin, L. A. Dunbar, R. Houdré, M. Mulot, and S. Anand, "Planar photonic crystals infiltrated with liquid crystals: optical characterization of molecule orientation," Opt. Lett. **31**, 1238–1240 (2006).
20. E.P. Kosmidou, E.E. Kriezis, and T.D. Tsiboukis, "Analysis of tunable photonic crystal devices comprising liquid crystal materials as defects," IEEE J. Quantum Electron. **41**, 657–665 (2005).
21. E.P. Kosmidou, E.E. Kriezis, and T.D. Tsiboukis, "Analysis of tunable photonic crystal directional couplers," J. Appl. Phys. **100**, 043118 (2006).
22. SOITEC website: http://www.soitec.com.
23. B. Bellini, M.A. Geday, N. Bennis, A. Spadło, X. Quintana, J.M. Otón, and R. Dąbrowski, "Design and simulation of single-electrode liquid crystal phased arrays," Opto-Electr. Rev. **14**, 269–273 (2006).
24. H. Desmet, K. Neyts, and R. Baets, "Modeling nematic liquid crystals in the neighborhood of edge," J. Appl. Phys. **98**, 123517 (2005).
25. R. Beccherelli, I.G. Manolis, and A. d'Alessandro, "Characterisation of photoalignment materials for photonic applications at visible and infrared wavelength," Mol. Cryst. Liq. Cryst **429**, 227–235 (2005).
26. A. Muravsky, "Photo-induced alignment technology for 3-D surface profiles of LCD substrates", Proc. LCP Conference (2006).
27. S.G. Johnson and J.D. Joannopoulos, "Block-iterative frequency-domain methods for Maxwell's equations in a planewave basis," Opt. Express **8,** 173–190 (2001), http://www.opticsexpress.org/abstract.cfm?URI=OPEX-8-3-173.
28. I. W. Stewart, "*The Static and Dynamic Continuum Theory of Liquid Crystals*," (Taylor & Francis, April 2004).
29. F. A. Fernández, S. E. Day, P. Trwoga, H. F. Deng, and R. James, "Three-dimensional modelling of liquid crystal display cells using finite elements," Mol. Cryst. Liq. Cryst. **375**, 291-299 (2002).
30. E. E. Kriezis and S. J. Elston, "Light wave propagation in liquid crystal displays by the 2-D finite-difference time-domain method," Opt. Commun. **177**, 69–77 (2000).
31. C. V. Brown, E. E. Kriezis, and S. J. Elston, "Rigorous analysis of the diffraction from a liquid crystal phase grating," J. Appl. Phys. **91**, 3495–3500 (2002).
32. W.C.L. Hopman, P. Potier, D. Yudistira, J. van Lith, P.V. Lambeck, R.M. De La Rue, A. Driessen, H.J.W.M. Hoekstra, and R.M. de Ridder, "Quasi-one-dimensional photonic crystal as a compact building-block for refratometric optical sensors," IEEE J. Sel. Top. Quantum Electron. **11**, 11–16 (2005).

1. Introduction

Several outstanding properties of photonic crystals (PhC) in all dimensionalities have been studied, revealed and demonstrated in the last 15 years (see for instance Ref. [1] and the special issue of Ref. [2]). Out of the PhC family, one-dimensional (1-D) PhC have attracted somehow less attention compared to their two- or three-dimensional counterparts, as they are in principle considered no more than well known Bragg gratings. However, numerous practical devices have been fabricated from 1-D PhC for optical communication and sensing systems (reflectors, filters, dispersion compensators), and many other functions are still to be exploited, nonlinear [3], superprism [4], slow light [5], and tunable properties [6]-[7] being some examples. As far as light guidance is concerned, in the plane normal to periodicity one can distinguish between in-

#77781 - $15.00 USD Received 4 December 2006; revised 17 January 2007; accepted 18 January 2007

variant material distribution (light is therefore unconfined, as in [8]), and boundary conditions that impose a transverse confinement (*i.e.* trenches throughout a slab waveguide [9], or fully etched Bragg gratings [10]). In the following we will consider structures of the second type. Therefore, the substrate should have the structure of a classical waveguide, for instance silicon-on-insulator, III-V heterostructure, free standing membranes or Si_3Ni_4 on silica. From the manufacturing point of view, most of the PhC implemented in integrated optics are fabricated by electron beam or deep UV lithography followed by reactive ion etching. Small, precisely defined features can thus be obtained. Nevertheless, limitations in the manufacturing technology result in roughness, especially on the sidewalls of the holes [11], and in non-verticality of the holes [12]-[13]. On the other hand, wet etching of silicon results in holes with very smooth sidewalls and well-controlled geometry as etching is nearly self stopping on the $\{111\}$ crystal planes [14]. However, very limited work has been devoted to wet etched PhC. Such studies most frequently focus on deep etching of (110) silicon, so that the resulting holes can be vertical [8]. In this paper we report the design and analysis of 1-D PhC fabricated by anisotropic wet etching of (100) silicon-on-insulator (SOI) wafers. To test feasibility, we have fabricated and characterized a preliminary sample of the silicon groove structure. In addition to being simple, this technology presents the practical merit of being developed for micromachining [15], microfluidics [16] and photonic integration [17]. Therefore, it becomes possible to infiltrate the PhC with a fluid material that may undergo changes in its optical properties under the dynamic control of external parameters, such as temperature or an electric field. Such a material can be for instance a nematic liquid crystal. Photonic crystal structures based on 2-D lattices, infiltrated with LC materials either in all holes or in a specific number of them (to generate specific defect modes) have already been discussed in the literature [18]-[21]. By analogy, the properties of the proposed 1-D SOI-based PhC structures may be controllably tuned when combined with a LC material. In this context, after evaluating the technological process and constraints, the paper theoretically studies the bandgap tuning of a novel 1-D PhC structure derived by anisotropic etching of SOI wafers. In a further approach, such 1-D PhC are also assessed as candidates for compact devices for optical filtering and refractometric sensing.

2. Key technological points

2.1. SOI wafers

SOI wafer geometry is characterized by the thicknesses of the top silicon layer and of the buried oxide layer. (100) SOI wafers are commercially available from SOITEC [22] with several choices of thickness for the top silicon layer and for the buried silicon dioxide (SiO_2). In the context of our optical studies, we have verified that a 1μm-thick SiO_2 layer is sufficient to fully optically isolate the silicon substrate.

2.2. Preferential etching of silicon

Depending on the chemical composition of the etching solution, monocrystalline silicon can be etched either isotropically (the etching rate is invariant along the crystallographic directions) or anisotropically (the etching rate does depend on the etching direction). In the latter case, specific crystallographic planes are exposed; it becomes possible then to produce a precise geometry with symmetries and homothetic properties. The most common etchants that induce preferential etching are alkaline solutions of potassium hydroxide (KOH), hydrazine, ethylenediamine-pyrocathecol (EDP), or tetramethyl-ammonium hydroxide (TMAH). The etching rate and the roughness after etching strongly depend on the concentration and the temperature of the solution. Haneveld *et al.* [14] have noted that a photoresist developer (OPD 4262, Olin) containing about 2.5% (in weight) of TMAH and undisclosed surfactants etches silicon at a slow etching rate of the order of 4 nm·min^{-1}. The etching procedure is standard and described in

#77781 - $15.00 USD Received 4 December 2006; revised 17 January 2007; accepted 18 January 2007

[17]. As the groove depth is small, we used a different product, Microposit MIF 319 developer (by Shipley) containing 2.5% wt of TMAH as well, operating at room temperature. The etching rate is 2.4 nm·min^{-1}. Figure 1 shows an atomic force microscope picture of a silicon rib etched on a monocrystalline silicon wafer. The rib top width is about 600 nm and thickness is 200 nm.

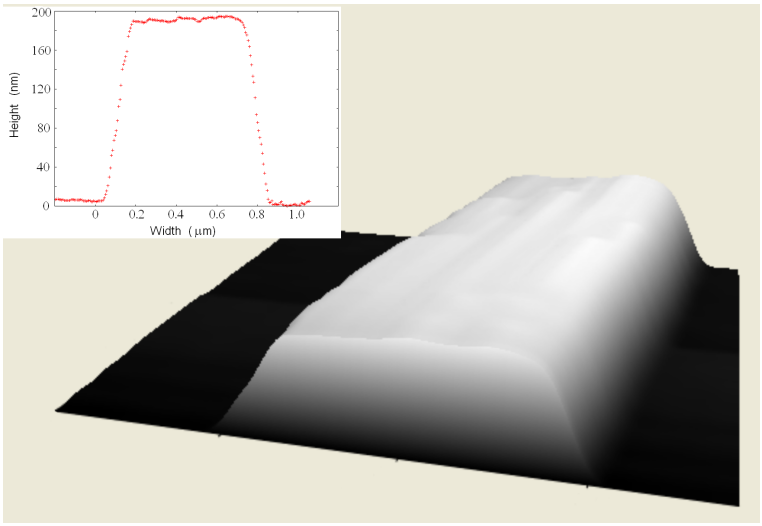

Fig. 1. Atomic force microscope picture of an etched silicon rib; height is 200 nm and the base width is 800 nm. The inset shows the transverse profile.

Measurements show that the roughness on the bottom and top silicon is in the order of few nanometers, typically between 2 nm and 4 nm. On SOI wafers though, the buried oxide acts as an etch stop, therefore the roughness on the bottom should be less. On the slanted sidewalls, the roughness is measured to be between 5 nm to 8 nm. The transverse profile permits to evaluate the sidewall angle, which is measured between 50° and 55° - the theoretical value being 54.7°. We have found that this angle is sensitive to the accuracy of the orientation of the wafer during lithography. The etched silicon rib of Fig. 1 demonstrates, in principle, the feasibility of fabricating well-defined silicon groove structures by the anisotropic wet etching technique proposed in the present study.

2.3. Liquid crystal

In order to achieve a wide tuning range, we consider high positive birefringence ($\Delta n = 0.38$), low viscosity nematic liquid crystals [23], characterized by ordinary and extraordinary indices of $n_o = 1.55$ and $n_e = 1.93$, respectively. The static dielectric anisotropy ($\Delta\varepsilon_r^{stat}$) of the liquid crystalline material equals 4.3, while the elastic constants can be fairly approximated by a value of $K = 10$ pN. By forcing reorientation out of a rest position, LCs present a choice of refractive indices with respect to the propagation of the optical field. Ideally this may continuously span between n_o and n_e. To our knowledge, no in-depth work exists on the alignment of liquid crystals in submicron grooves. Desmet et al. [24] reported a numerical study of the orientation along a right-angle silicon edge without alignment layer, and predicted a molecular alignment along the edge. Muravsky [26] has presented the study of a nematic liquid crystal alignment layer on a textured wafer.

#77781 - $15.00 USD Received 4 December 2006; revised 17 January 2007; accepted 18 January 2007

3. Structure layout

In order to estimate the PhC properties of the 1-D proposed structures, we perform an analysis originating from two main classes of structures: (i) the first one is a reference structure (Fig. 2(a)) based on vertically-etched sidewalls (after a dry-etching process, or wet etching on (110) silicon), and (ii) the second one accounts for slanted walls as obtained by a wet-etching process of (100) silicon (Fig. 2(b)), along the lines of the structure shown in Fig. 1.

The material inside the grooves can be air, polymer or liquid crystal. The substrate is the 1μm SiO_2 layer of SOI, and the superstratum is either glass or the same materials as it is in the grooves; both layers are considered to extent to infinity in terms of optical calculations. Structures derived from the generic layout of Fig. 2(b) are foreseen to accommodate and exhibit a number of particular features related to their fabrication: (a) the wet-etching process along the particular crystallographic direction is self-stopping and results in more well-defined structures with smooth boundaries, as already demonstrated in principle in Fig. 1, (b) fabrication is simpler and more-tolerant to errors, and (c) LC alignment is facilitated in such geometry as compared to the counterpart of Fig. 2(a), in particular when photo-alignment techniques are employed [25]-[26] or well-developed vacuum-based SiO_x deposition techniques.

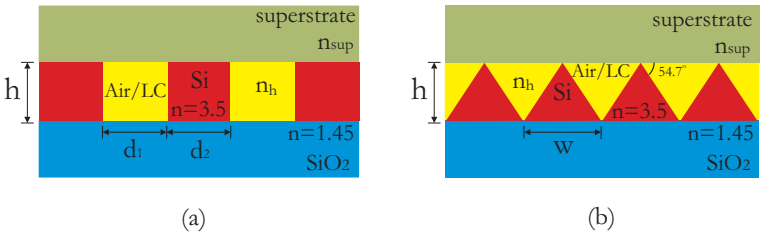

Fig. 2. One-dimensional photonic crystal based on (a) vertical walls, and (b) a grooved structure with slanted walls inclined at 54.7°, resulting from anisotropic wet etching of (100) silicon. The thickness h of the silicon slab is 220 nm.

4. Numerical optical studies

In the following, we consider a SOI wafer by SOITEC whose nominal silicon layer thickness is 220 nm. The refractive indices of Si and SiO_2 for the wavelength range here studied ($1.3\mu\text{m}< \lambda < 2.3\mu\text{m}$) are considered to be 3.5 and 1.45, respectively. The device of Fig. 2(a) for a filling factor equal to 50% (d_1=d_2), and $n_{sup} = n_h = 1.0$ demonstrates a TE bandgap between 0.194 and 0.304 in normalized units of w/λ ($w = d_1 + d_2$), as calculated using a freely available planewave expansion model [27]. It should be mentioned that this is the first (lowest frequency) TE bandgap, which lies below the light line, *i.e.* it refers to truly guided and not radiating modes; our analysis hereinafter focuses on the study of the properties of this bandgap. The term TE follows the slab waveguide terminology, namely the electric field is perpendicular to the plane shown in Fig. 2.

With respect to the device of Fig. 2(b), considering a 50% filling factor as well and the presence of air above and in the grooves, the corresponding TE bandgap in normalized units was calculated between 0.2 and 0.258, using the same planewave expansion method [27] as in the case of the vertical wall structure. Although the presence of the slanted walls negates the uniformity of the vertical trenches of Fig. 2(a) and subsequently leads to a shrinkage of the bandgap, the resulting gap-width is still significant; for the silicon slab thickness here considered ($h = 220$ nm), the PhC period is $w = 2h/\tan(54.7^\circ) \simeq 311$ nm, which translates into a bandgap from 1205 to 1555 nm.

#77781 - $15.00 USD Received 4 December 2006; revised 17 January 2007; accepted 18 January 2007

4.1. *Nematic LC director orientation*

In order to predict the behavior and performance of LC infiltrated photonic crystal structures, it is necessary to calculate the response of the nematic material to the application of an external field. The exact configuration of the nematic director in a confined geometry can be resolved via the minimization the Oseen-Frank free elastic energy over the material's bulk, and the solution of the resultant Euler-Lagrange differential equation [28]-[29]. Our calculations were performed under the assumption of a uniform electric field oriented perpendicularly to the substrate.

As a reference problem, we first analyzed the structure shown in Fig. 3(a), that is a triangular groove etched in a 220 nm thick silicon slab. The electric field necessary for tuning the director orientation is applied between an ITO layer, which is placed upon the silicon slab, and the bottom conductive silicon. For clarity reasons, the buffer layer which optically isolates the ITO layer from the guiding region, in order to suppress light absorption, is not shown in the illustration. We consider that the molecules which are adjacent both at the groove's walls and the top surface lie parallel to the groove's axis (homogeneous strong anchoring conditions). In the absence of any field, the nematic director is everywhere parallel to the groove's axis. The application of an electric field tilts the LC molecules in the (yOz) plane, and leads to the formation of a director pattern, characterized locally by the tilt angle (θ). As the field intensity raises, the tilt angle tends towards 90^o in the free bulk of the groove, while remaining zero at the anchored surfaces. This behavior may be observed in the tilt angle profiles shown in Fig. 3(b) for three increasing field intensity values, properly selected so as to illustrate in an indicative manner the progressive switching of the LC material.

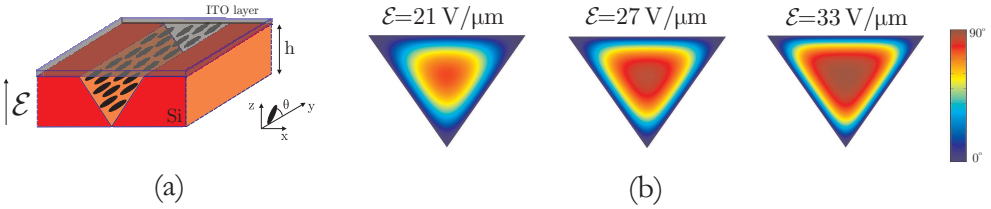

Fig. 3. Nematic director tuning in a triangular groove etched in silicon: (a) structural layout, and (b) distribution of the tilt angle (θ) under the application of an electric field for $E = 21$, 27, and 33 $V/\mu m$.

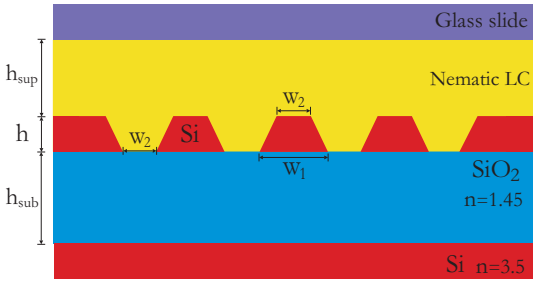

Fig. 4. One-dimensional photonic crystal design based on SOI etched grooves. The thicknesses of the silicon slab and the SiO_2 substrate are $h = 220$ nm and $h_{sub} = 1\mu$m, respectively; the parameters w_1 and w_2 equal 370 and 50 nm, and the photonic crystal period is $d = w_1 + w_2 = 420$ nm. The grooves are infiltrated with a nematic LC material which also forms a residual overlayer of thickness h_{sup}

#77781 - $15.00 USD Received 4 December 2006; revised 17 January 2007; accepted 18 January 2007

In order to provide a means of controlling the photonic crystal's period, and thus its optical response, we have also treated a more general structure, which is shown in Fig. 4. The trenches in this case are trapezoidal in shape, and the structure's period equals the sum of the trapezoid's bases $w_1 + w_2$; here we consider a period of 420 nm, with $w_2 = 50$ nm. Another degree of freedom is also introduced, in order to account for a possible residual layer of LC material during the infiltration procedure, whose thickness is denoted by h_{sup}. The electric field in this case as well is applied between an ITO electrode placed above the residual LC layer (and optically isolated from the guiding region by a buffer), as shown in Fig. 5(a), and the bottom conductive silicon. Homogeneous strong anchoring conditions are assumed at the Si/LC boundary and the top surface, while periodic boundary conditions are applied at the sidewalls. The evolution of the tilt angle profile over the groove's section for an indicative set of increasing intensity values is presented in Fig. 5(b), for $h_{sup} = 0.5\mu m$; tilting of the LC molecules in the residual layer is more effective than in the region inside the groove, where they are restricted by the anchoring conditions. This also accounts for the fact that similar levels of reorientation are achieved in the trapezoidal groove case for lower values of the applied electric field, as compared to the triangular case (see Fig. 3(b) and Fig. 5(b)).

A more detailed analysis regarding the tuning effectiveness for both the triangular and the trapezoidal groove structures is presented in the diagrams of Fig. 6. For an ample range of electric field intensity values E, the average tilt angle θ_{av} is calculated in order to provide a measure of the overall tuning capacity. It should be stressed that this averaging is calculated only over the region within the grooves, since this is the part of the LC material that plays a critical role in the generation of the PhC bandgap. Figure 6(a) shows the dependence of θ_{av} over the field intensity. The flattened bottom of the trapezoidal groove smooths up to a certain extent the anchoring stress as compared to its triangular counterpart, hence improving its tuning response. As the residual LC overlayer raises in thickness, the upper boundary moves away from the silicon slab, relaxing the anchoring condition at the groove's top surface; thus, for the same intensity value, tuning is more enhanced in this case than in the absence of the residual layer. Furthermore, for adequately high intensity values, the tilt angle at the groove's top surface reaches values very close to 90°, hence the convergence of the curves corresponding to h_{sup} =0.1, 0.5, and 1 μm in the high intensity region of the diagram in Fig. 6(a).

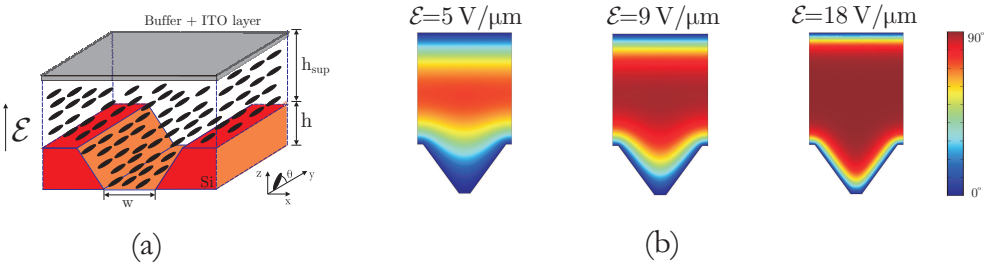

Fig. 5. Nematic director tuning in a trapezoidal groove etched in Si: (a) structural layout, and (b) distribution of the tilt angle (θ) under the application of an electric field for $E = 5$, 9, and 18 $V/\mu m$, for an overlayer thickness of $h_{sup} = 0.5\mu m$.

Since the curves of Fig. 6(a) refer to structures of different overall thickness ($h_{sum} = h + h_{sup}$), the voltage drop $\Delta V = Eh_{sum}$ across the optically active LC layer differs among the examined cases. Figure 6(b) shows the dependence of θ_{av} over the dropped voltage values that correspond to the curves plotted in Fig. 6(a). This interpretation, which considers the values of voltage drop as a point of reference, might provide more direct insight in terms of practical applications, in case, for instance, where the applied voltage is restricted below a limited value, due to material

#77781 - $15.00 USD Received 4 December 2006; revised 17 January 2007; accepted 18 January 2007

constraints (e.g. dielectric breakdown), or manufacturing considerations (power dissipation, compatibility issues, etc.). In all cases examined, the threshold value needed to primarily induce the response of the LC molecules remains around 2.5 V, despite the increase of the overlayer thickness; this observation may be parallelized with the fact that the threshold voltage value in a simple nematic LC cell is independent of the cell's thickness. In terms of tuning efficiency, results show that in principle the best response for the cases studied is achieved for an overlayer thickness value of 100 nm. Such a small value seems to favorably compensate the increase of the overall cell thickness with the relaxation of the anchoring strength at the groove's top; on the contrary, for higher values (0.5 and 1 μm) the tuning efficiency is substantially undermined as shown in Fig. 6(b). As a conclusive remark, for zero or small values of h_{sup} significant tuning can be achieved for relatively low values of voltage: θ_{av} is almost 70° for $\Delta V = 10$ V.

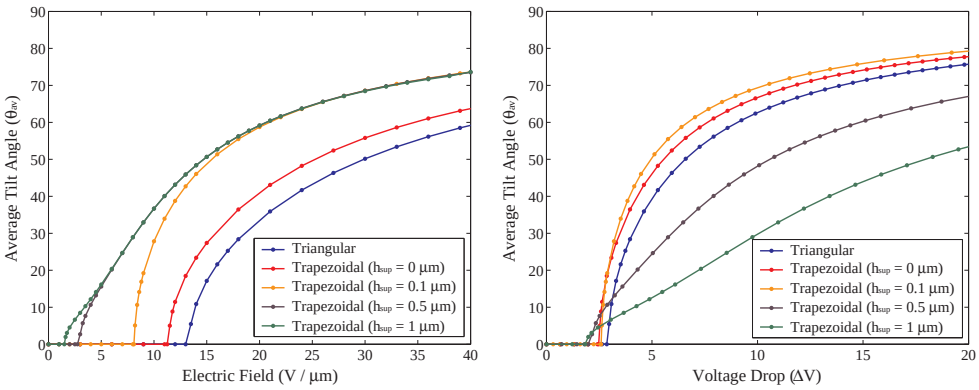

Fig. 6. Average tilt angle (θ_{av}) over the groove's cross-section for the structures shown in Figs. 3(a) and 5(a), in terms of: (a) applied field intensity and (b) dropped voltage.

4.2. Band-edge tuning

The bandgap tuning properties of the structure proposed in Fig. 4 were investigated by means of a fully anisotropic finite-difference time-domain (FDTD) analysis [30]-[31]. The director patterns calculated after the minimization of the free elastic energy within the grooves were introduced in a custom FDTD code capable of dealing with anisotropic materials, while the computational domain was backed by the material independent perfectly matched layer. The grid was excited with the fundamental TE mode supported by the silicon slab; given its thickness ($h = 220$ nm), this slab supports only one TE mode in the telecom wavelength range. The power transmission calculated at the waveguide's output for the PhC structures was normalized with respect to the transmission of an unpatterned silicon slab waveguide.

Figure 7 shows the bandgaps for different values of the applied electric field for a 6-period structure of trapezoidal grooves, as shown in Fig. 4, where we assume no residual LC overlayer ($h_{sup} = 0$). The superstrate in terms of the calculations is characterized by an index of 1.45 (glass slide). For $E = 0$ V/μm, all LC molecules lie along the groove's axis; thus, the TE polarized field senses a uniform material in the groove with an index of $n_e = 1.93$. As the field intensity increases, significant tuning is achieved and the bandgap progressively broadens. The observed bandgap tuning follows as a result of the switching of the LC material in the groove, which is estimated by the red curve in Fig. 6(a). The high-frequency band-edge is shifted by more than 75 nm as the value rises from 0 to 54 V/μm (ΔV from 0 to 12 V), while power transmission

#77781 - $15.00 USD Received 4 December 2006; revised 17 January 2007; accepted 18 January 2007

at 1550 nm drops from 0.686 for $E = 0$ V/μm down to 0.046 for $E = 54$ V/μm (an extinction ratio of 11.7 dB).

The impact of the thickness of the residual LC overlayer that may be present after the infiltration of the grooves as a consequence of manufacturing imperfections is assessed in Fig. 8. In order to provide a more practical interpretation, transmission curves of the photonic crystal for various values of h_{sup} were calculated, assuming a constant voltage drop equal to $\Delta V = 5$V. As presented in Fig. 8, the shifting of the bandgap's high-frequency edge is comparable for the ideal case of zero overlayer and that for $h_{sup} = 100$ nm. Nevertheless, as h_{sup} grows larger, the bandedge shifting is significantly suppressed, due to the respective reduction of the LC switching efficiency as demonstrated in Fig. 6(b). Although it seems that a very thin residual layer does not severely undermine the tuning capacity of the structure, in practice the overlayer's thickness should be better kept as low as possible. The addition of such a LC overlayer raises the overall thickness of the optically active region (and the corresponding voltage drop needed to achieve tuning of the LC molecules in the grooves), without notably contributing in the bandgap formation, since this extra LC material is superposed above the photonic crystal structure.

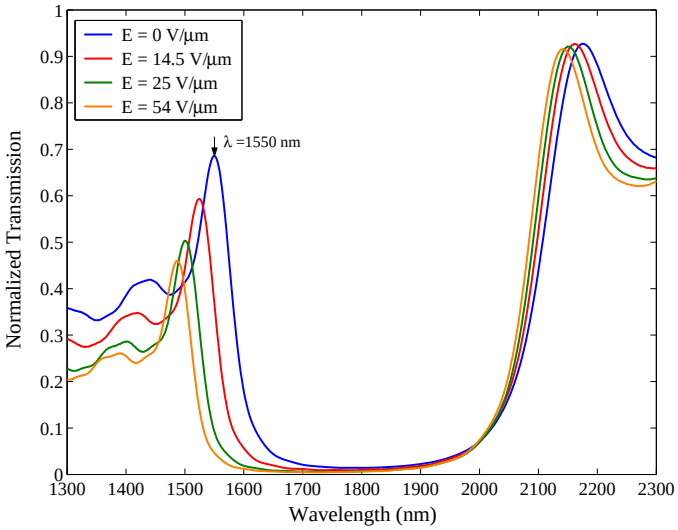

Fig. 7. Band-edge tuning for different values of electric field intensity, for the structure shown in Fig. 4. The LC overlayer thickness is zero and the refractive index of the glass slide equals 1.45.

In order to associate the bandgap formation with the nematic director patterns that correspond to different field values in a more systematic manner, a comparison was initially made between results obtained by runs with LC director patterns (for h_{sup}=0) and the corresponding results for a PhC structure where the grooves are assumed to be filled with a uniaxial anisotropic material, with its axis fixed along the direction indicated by the average tilt angle of the realistic LC patterns. The results are shown in Fig. 9; the curves calculated with a fixed tilt angle provide a relatively fair approximation in terms of defining the bandgap edges. Hence, from measurements of the bandgap tuning of real devices, one can understand in principle the behavior of LC confined in such submicron geometries. This may provide answers to fundamental surface and volume physics of LCs.

As a further step towards the characterization of the device, a bandgap reference map was

#77781 - $15.00 USD Received 4 December 2006; revised 17 January 2007; accepted 18 January 2007

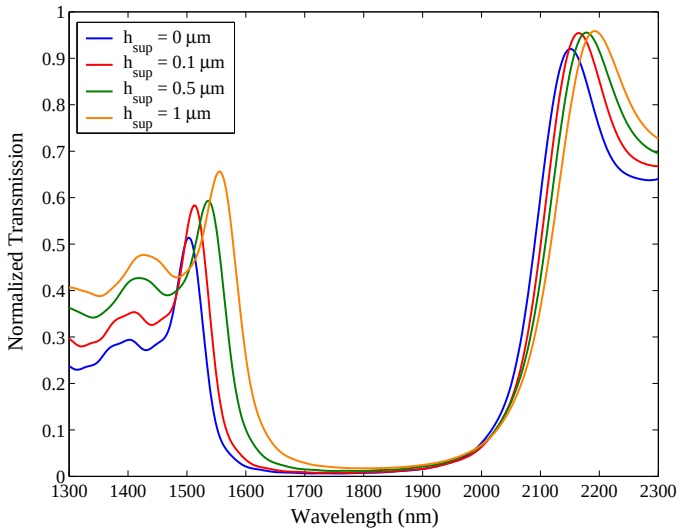

Fig. 8. Band-edge tuning for a constant value of voltage drop ($\Delta V = 5$V) for different values of the thickness of the residual LC overlayer, for the PhC structure of Fig. 4.

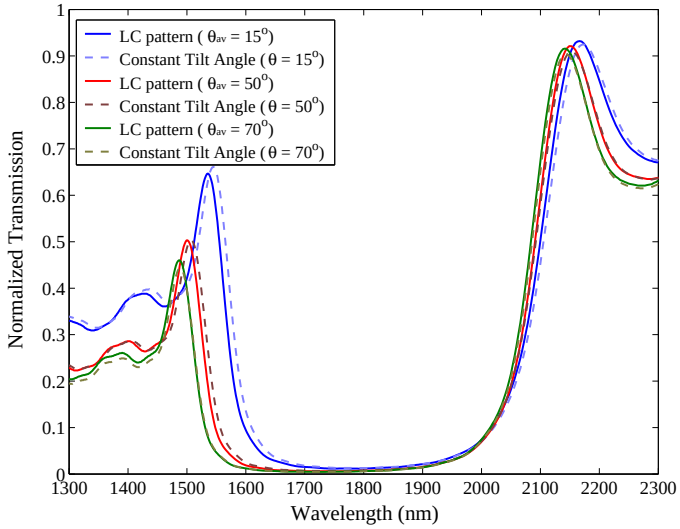

Fig. 9. Band-edge tuning comparison between calculations invoked for realistic nematic director profiles such as those depicted in Fig. 5, and constant tilt angles corresponding to the averaged angle (θ_{av}) of these profiles.

created by calculating the transmission curves for the structure, assuming that the grooves are filled with an isotropic fluid with an index varying between n_o=1.55 and n_e=1.93. Afterwards, anisotropic FDTD runs were carried out for a series of realistic nematic patterns corresponding to averaged tilt angles θ_{av} between 0 and 90°, and for uniaxial materials with fixed tilt angles of equal value. Each transmission curve obtained was optimally matched to one of the set of reference curves corresponding to an equivalent isotropic index ($n_{iso,eq}$) by calculating a minimum least square error. The final results associating the bandgap properties of an anisotropic

#77781 - $15.00 USD Received 4 December 2006; revised 17 January 2007; accepted 18 January 2007

structure with the equivalent isotropic index filling the grooves are shown in Fig. 10. It can be observed that the average tilt angle curve provides a fair approximation for the curve obtained for the various realistic LC patterns, especially for large angles, although it always tends to underestimate the tuning efficiency, which accounts for the relative difference with respect to the n_e value. It seems that the presence of a highly tilted core within the groove (as depicted in Fig. 3(b)) plays a more significant role in the bandgap formation than the anchored surfaces; the substitution of this specific nematic director modulation in the grooves with an averaged tilt value tends to a slight underestimation of the resulting bandgap's width.

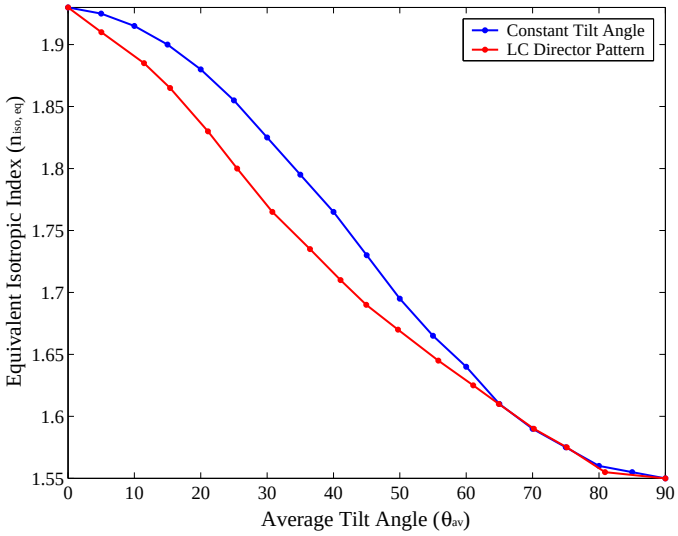

Fig. 10. Mapping of the bandgap response to an equivalent isotropic index filling the grooves for different realistic nematic director patterns and corresponding results when considering a constant tilt angle equal to the average value.

4.3. Refractometric optical sensing

By substituting the LC with another fluid that may experience a variation of its refractive index under an external stimulus or the modification of certain parameters or conditions, the photonic crystal structure under study may also be used as a sensor, similar to [32]. Figure 11 shows the layout of such a refractive index sensor device; both the grooves and the superstratum are covered with a measurand isotropic fluid whose index is denoted as n_s. In order to provide efficient performance, a sensor device should ideally be capable of measuring small variations of the refractive index in a wide dynamical range. In an attempt to evaluate the sensing capability of the proposed PhC, we plot at first in Fig. 12(a) a family of curves depicting the normalized transmittance coefficient of the PhC structure studied in 4.2 for a given index range of the measurand fluid ($1.6 < n_s < 1.9$), where the thickness of the fluid overlayer is considered to be infinite. We have observed that for an overlayer thickness of more than 0.5 μm the results are not notably affected, since light is mainly confined in the silicon slab; thus, the exact value of the overlayer in practical applications in not expected to play a critical role, as long as it exceeds a threshold value of $\approx 0.5\mu$m. Optimum sensing efficiency is expected at wavelengths where transmission is greatly affected by small changes of n_s. It can be derived from Fig. 12(a) that the sensing wavelength should be chosen in the range of the high frequency band-edge shifting. Here we have chosen a testing wavelength of 1579 nm. Using the definition of sensitivity S given in [32]

#77781 - $15.00 USD Received 4 December 2006; revised 17 January 2007; accepted 18 January 2007

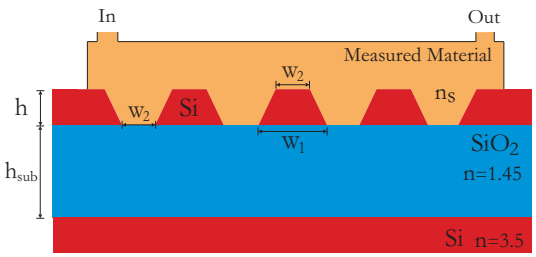

Fig. 11. Refractive index sensor based on the design of Fig. 4. The grooves as well as the superstrate region is covered by the measurand fluid characterized by an index of n_s. Other parameters follow the values mentioned in Fig. 4.

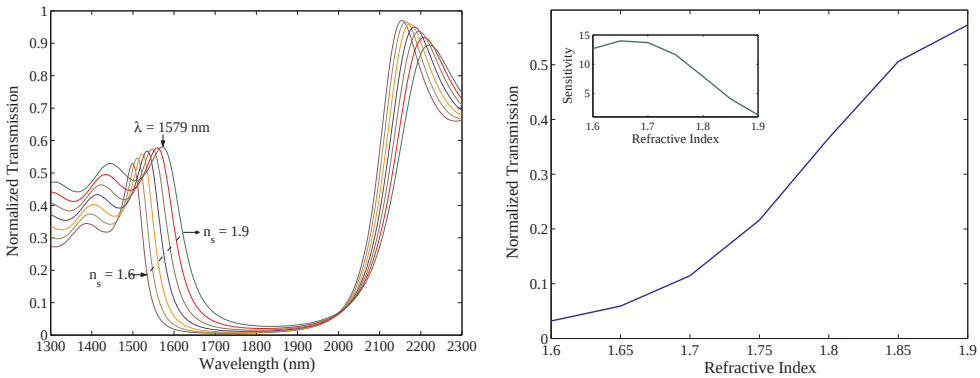

Fig. 12. Sensitivity of the power transmission coefficient of the proposed one-dimensional photonic crystal slab: (a) transmission curves as a function of the superstrate (measurand fluid) refractive index and (b) transmission versus the change in the superstrate index (n_s) calculated at 1579 nm, and (inset) dependance of the associated sensibility S over n_s.

$$S = \frac{1}{P}\frac{\partial P}{\partial n_s}, \tag{1}$$

where P is the transmitted power and n_s the refractive index of the measurand fluid. Figure 12(b) shows the changes in transmission for the trapezoidal groove PhC structure, as well as the sensitivity of the sensor at 1579 nm over the refractive index n_s. The sensitivity slightly varies around a mean value of approximately 12 in the range $1.6 < n_s < 1.75$. For a simple photodetector setup with a resolution η of 0.1% in power detection, the minimum detectable cladding index change in this case is assessed to be $\Delta n = \eta/S \simeq 8\times10^{-4}$. It should be mentioned that the response of the sensor in this dynamical range, which covers a total index change of about 0.15, is almost linear. To compare this result with the sensitivity demonstrated in classical resonators, we have calculated that a Fabry-Pérot cavity with $R = 0.9$ mirrors and thickness $d = \lambda/(2n_o)$ can yield higher levels of sensitivity, but within a smaller range ($S > 20$ for $1.51 < n < 1.59$, with sensitivity dropping in a wider range) and exhibiting a less linear behavior. Moreover, given that the bandgap formation mechanism is more or less similar for different refractive indices of the isotropic material filling the grooves, similar performance should also be expected for different ranges of n_s, by properly selecting a wavelength around the corresponding band-edge shifting regime. Further improvements in the minimum detectable signal should be

#77781 - $15.00 USD Received 4 December 2006; revised 17 January 2007; accepted 18 January 2007

possible by using synchronous (lock-in based) acquisition techniques. Finally, the proposed slanted geometry is also expected to ensure smoother flow of the measurand material along the grooves, as well as to facilitate the necessary procedure to rinse the structure in order to blank/reset the sensor, as compared to its vertical wall based counterpart.

5. Conclusion

We have exploited the micromachining properties of silicon to design a novel PhC structure, made to ease the fabrication process and achieve smoother surfaces. The nematic director orientation in submicron grooves etched in silicon has been extensively studied. A PhC based on this kind of structure exhibits a photonic bandgap for TE polarized light. By infiltrating it with a nematic LC, we demonstrated a tunability of more than 75 nm for the air band-edge, with an extinction ratio of about 12dB. The tuning properties of such structures were studied in a systematic way, in order to provide a rapid association of the applied electric field voltage with the resulting bandgap properties of the photonic crystal. In a reverse approach, from the bandgap-edge tuning one may deduce valuable information of the LC orientation, when confined in submicron grooves. Finally, the same structure was also studied in the context of refractometric optical sensing applications. A quasi-linear response to refractive index changes with satisfactory sensitivity levels was calculated for a wide dynamical range.

Acknowledgements

The authors acknowledge the financial support of the Italian Ministry of Foreign Affairs.

#77781 - $15.00 USD Received 4 December 2006; revised 17 January 2007; accepted 18 January 2007